Proceedings of the 2024 14th International Pipeline Conference
IPC 2024
September 23-27, 2024, Calgary, Alberta, Canada

IPC2024-134010

CONSTRAINT-INDEPENDENT CONSTANT CTOA DETERMINATION FOR DUCTILE STABLE CRACK GROWTH

Xian-Kui Zhu
Materials Technology and Energy Science
Savannah River National Laboratory
Aiken, SC 29808, USA

ABSTRACT

Crack tip opening angle (CTOA) has been used as a reliable fracture toughness parameter for decades to characterize stable ductile crack growth for thin-walled aerospace structures in the low-constraint conditions. Recently, the CTOA parameter was also applied to the pipeline industry, and a CTOA test standard ASTM E3039 was thus developed for testing a critical constant CTOA. Research showed that the constant CTOA can reasonably describe fracture toughness required to arrest a dynamic crack propagation for a modern gas pipeline. However, the CTOA fracture criterion requires constraint-independent CTOA toughness against stable ductile crack growth.

ASTM E3039 recommends a drop weight tearing test (DWTT) specimen for CTOA testing. Since a shallow crack is used, DWTT measured CTOA may depend on constraint level at the crack tip. To understand if it is the case, this paper evaluates the critical CTOA for a set of fracture toughness tests on single edge notched bend (SENB) specimens with shallow and deep cracks based on four CTOA estimation models. In which, the Ln(P)-LLD linear fit model is similar to that used by ASTM E3039 in the CTOA calculation. Fracture test data for X80 pipeline steel and HY80 structural steel are considered in the CTOA evaluation. The results show that the four CTOA models can determine a crack size-independent constant CTOA over stable ductile crack growth for the SENB specimens. As a result, CTOA determined by ASTM E3039 is constraint-independent and transferable to use for an actual crack propagating in a gas pipeline.

KEYWORDS: fracture arrest toughness, Constant CTOA, CVN, DWTT, SENB specimen

1. INTRODUCTION

Fracture mechanics methods have been extensively applied to engineering design, crack assessment, and structural integrity management for large-scale infrastructure in the energy sector, including nuclear or petrochemical pressure vessels, energy storage tanks, and oil & gas transmission pipelines. Most pressure vessels are made of stainless steels, and pipelines are made of carbon steels. For these ductile steels, the elastic-plastic fracture mechanics methods are usually used in an engineering critical analysis (ECA) or crack assessment, where fracture toughness is described by one of fracture parameters: J-integral [1], crack tip opening displacement (CTOD) [2], and crack tip opening angle (CTOA) [3]. Initially, the J-integral was proposed to describe the intensity of singularity of crack-tip field, CTOD was proposed to describe the capability of crack opening, and CTOA was introduced to simulate stable crack growth for finite element analysis (FEA). Since the 1980s, these fracture parameters have been used to characterize fracture toughness of ductile steels against crack initiation or stable growth. Over the past decades, many fracture toughness test methods have been developed and standardized by American Society for Testing and Materials (ASTM) for metallic materials, as reviewed by Zhu and Joyce [4]. Compact tension (CT) and single edge notched bend (SENB) specimens are two commonly used standard fracture test specimens. ASTM E399 [5] was developed for testing the plane strain fracture toughness K_{IC}, and ASTM E1820 [6] was developed for testing plane strain initiation toughness or resistance curves in terms of the J-integral and CTOD. For non-standard fracture specimens, Zhu [7] presented a technical review on the fracture toughness test methods.

The J-integral and CTOD are usually used to describe crack initiation and small stable crack growth, and CTOA can be used to characterize large stable crack growth for ductile steels. In fact, CTOA has been used for decades as a reliable fracture toughness parameter to characterize stable ductile crack growth for thin-walled aerospace structures in the low-constraint conditions [8]. In 2006, ASTM developed the first CTOA test standard E2472 [9] for thin-walled CT and middle-crack tension (MT) specimens, where CTOA is directly measured on the specimen surfaces using a surface measurement technology, such as digital image correction [10] or optical measurement methods [11]. In recent years, the pipeline industry started to use the constant CTOA as an arrest fracture toughness parameter to control and prevent a dynamic crack propagation in modern gas pipelines [12 – 18]. Note that a typical wall thickness may be less

This work was produced by Battelle Savannah River Alliance, LLC under Contract No. 89303321CEM000080 with the U.S. Department of Energy. Publisher acknowledges the U.S. Government license to provide public access under the DOE Public Access Plan (http://energy.gov/downloads/doe-public-access-plan).

than 5 mm for an aerospace structure but can be 6.5 mm to 20 mm for a gas pipeline. As such, a surface CTOA measured using ASTM E2472 [9] may be not applicable to gas pipelines due to thicker walls. Experiments have shown that CTOA measured at the midplane of a fracture specimen can be significantly smaller than surface CTOA for a thicker specimen [19-20]. Thus, a constant midplane CTOA would be more appropriate to use for gas pipelines. To this end, Martinelli and Venzi [21] developed an approximate model for estimating CTOA from the post-peak absorbed energy that was calculated from the load-displacement data measured from a single SENB specimen test. After modification, Xu et al. [22] proposed a simplified single specimen method that can infer more accurate CTOA using load-displacement data from a thicker drop weight tear test (DWTT) specimen. On this basis, ASTM developed a second CTOA test standard E3039 [23] in 2016 for determining a constant CTOA for ferritic steels at the midplane of DWTT specimen. This DWTT specimen has a shallow crack, corresponding to the low-constraint condition at the crack tip. Without further study, it is unknown if the ASTM E3039 measured CTOA is constraint-dependent or not.

This paper attempts to evaluate the constraint-independence of CTOA determined from quasi-static fracture toughness tests on SENB specimens with shallow and deep cracks in different constraint conditions at the crack tip. Four CTOA estimation models are introduced for determining a constant CTOA over stable crack growth in the SENB testing. Among them, the ln(P)-LLD linear fit model is similar to that used by ASTM E3039 for calculating CTOA for DWTT specimens. A set of fracture test data for SENB specimens with different crack sizes in X80 and HY80 steels are considered in the CTOA evaluation. The results show that the proposed CTOA models can determine crack size or constraint-independent, constant critical CTOA values over stable crack growth in the SENB specimens. This infers that CTOA measured by ASTM E3039 is constraint-independent and transferable to use for an actual crack propagating in a gas pipeline.

2. CTOA STANDARD TEST METHODS

2.1. CTOA definition

CTOA is referred to as the angle between two crack faces of a crack starting from the crack tip. Due to large blunting at the crack tip, the original straight crack faces become curved during large plastic deformation of ductile steels. Accordingly, the CTOA is simply defined as an angle, ψ, that corresponds to the total CTOD (i.e., δ) at a given distance *d* from the crack tip in the order of 1 mm, as shown in Fig. 1. From this figure, CTOA or ψ is mathematically defined by:

$$\psi = 2\arctan\left(\frac{\delta}{2d}\right) \tag{1}$$

If ψ is less than 20°, Eq. (1) can be simplified and approximated as ψ = δ/d with an error less than 1%.

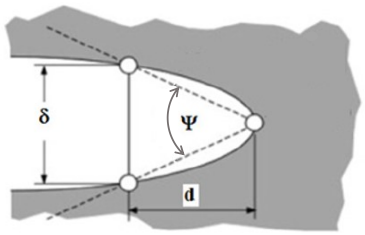

Figure 1. Definition of CTOA at a curved crack tip.

2.2. CTOA standard test method - ASTM E2472

In 2006, ASTM published the first CTOA standard test method E2472 [9] for measuring fracture resistance to stable crack extension in metallic materials for thin-walled specimens under the low-constraint conditions, where both crack length and ligament size are larger than wall thickness with a factor of 4, i.e., a/B ≥ 4 and b/B ≥ 4. This CTOA standard is a direct surface measurement method and determines a constant critical CTOA over stable crack growth using a CT or MT specimen. Both thin-sheet CT and MT specimens require anti-buckling guides during CTOA testing. ASTM E2472 [9] determines an averaged CTOA from Eq. (1) using the four-point approach within the minimum and maximum crack extensions.

To provide a longer uncracked ligament for a longer stable crack growth, different thin-walled bending specimens, such as modified double cantilever beam [MDCB] [11] and DWTT [24], were utilized to measure CTOA for pipeline steels in guidance of ASTM E2472 [9]. The test results showed that these two specimens determined comparable CTOA values. Xu et al. [24] further pointed out that DWTT specimens are suitable for a mill test, while MDCB specimens are more suitable for a laboratory test in supporting the DWTT CTOA testing.

2.3. CTOA standard test method – ASTM E3039

In 2016, ASTM developed a second CTOA standard test method E3039 [23] for measuring fracture propagation toughness in terms of steady-state CTOA using the DWTT specimens. The method is applicable to ferritic steels that exhibit predominantly ductile fracture with at least 85% shear area. This CTOA test standard may meet the technical needs to improve the CVN-based fracture control technology for managing modern gas pipelines. The critical CTOA is defined at the midplane (B/2) of DWTT specimens and calculated by:

$$CTOA_{\frac{B}{2}} = \frac{8r_p}{\xi}\frac{180}{\pi}\ (degree) \tag{2}$$

where r_p is the rotation factor and ξ is the absolute value of the slope of $\ln(P/P_m)$ versus $(\Delta-\Delta_m)/S$ curve, all data corresponding to $\ln(P/P_m)$ values between -0.5 to -1.2. Here, P_m is the maximum applied force, and Δ_m is the load-line displacement (LLD) at P_m. The crack steady-state region assumes to occur between P/P_m = 0.60 and P/P_m = 0.30.

Note that the rotation factor is an approximate constant of 0.55, but more accurately it is a function of specimen thickness,

yield strength and Charpy impact energy [23]. Numerical analysis [19] showed that the CTOA values derived from Eq. (2) are in good agreement with the values of $CTOA_{B/2}$ calculated at the midplane of the DWTT specimen. This midplane $CTOA_{B/2}$ is different from surface CTOAc defined in ASTM E2472 [9].

2.4. Constant CTOA simulation

In addition to the CTOA test methods and experimental studies, extensive elastic-plastic FEA simulations were also performed to investigate constant CTOA for ductile steels [20, 25-26]. FEA simulations can determine more accurate CTOA over stable ductile crack growth for different fracture specimens such as CT, SENB, MT, MDCB and DWTT. Once the constant CTOA toughness and a crack driving force in terms of CTOA are obtained for a given crack, the crack stability can be assessed using the CTOA fracture criterion. The objective of this work is to determine constraint-independent, constant CTOA toughness rather than a CTOA crack driving force.

3. CTOA ESTIMATION USING SENB SPECIMENS

Both SENB and DWTT are three-point bending specimens, but an SENB has smaller specimen sizes than a DWTT. For a same shallow crack ratio, these two bending specimens may have the similar mechanics behavior at the crack tip, such as constraint conditions and stable constant CTOA at the midplane. This section introduces four indirect estimate methods to evaluate midplane CTOA from fracture toughness testing on SENB specimens in the plane strain condition.

3.1. CTOA estimation from load-displacement data

Recently, Zhu et al. [27] developed three CTOA estimation methods from the load-LLD data for SENB specimens based on the plastic hinge model, as adopted by BS 7448-1 [28]. Figure 2 illustrates the plastic hinge model for an SENB specimen with a growing crack, where a small LLD increment, dΔ generates a small crack extension, da, and makes each specimen arm to rotate a small angle, dθ. This results in a small CTOD increment, dδ, at the crack tip. The distance from the crack tip to the rotation center is denoted as $r_p b$, here $b = W-a$ is the ligament size and r_p is the plastic rotation factor. For standard SENB specimens with a deep crack in the range of $0.45 \le a/W \le 0.70$, $r_p = 0.44$ [28]. For shallow cracked SENB specimens, r_p may depend on crack size and strain hardening rate of steels [4]. This may need further study if necessary.

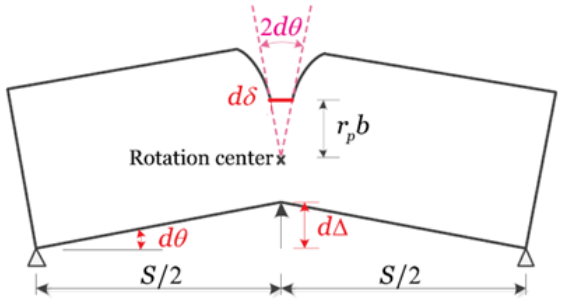

Figure 2. Plastic hinge model for an SENB specimen.

The rigid plastic model assumes that the material is perfectly plastic. For an SENB specimen at post yielding, applied load can be approximated as limit load for the perfectly plastic material:

$$P = \frac{\lambda \sigma_f B (W-a)^2}{S} \tag{3}$$

where λ is a dimensionless constant, σ_f is the flow stress with the average of yield strength and ultimate tensile strength, B is the specimen thickness, W is the specimen width, a is the crack length and S is the span of the beam. Note that λ = 1.455 for SENB specimens in the perfectly plastic material under the plane strain conditions. For a strain hardening material, λ may depend on the strain hardening exponent of the material. In a fracture test, both applied load and crack length are recorded, and thus λ can be estimated from the test data and Eq. (3).

From Fig. 2, the following geometrical relations are obtained:

$$d\theta = \frac{d\Delta}{S/2} \tag{4}$$

$$d\delta = 2 r_p b d\theta \tag{5}$$

When the crack grows for a small increment, da, CTOD increases a small amount of dδ that corresponds to CTOA at the current crack tip. This can be illustrated in Fig. 1, where d is replaced by da, and δ is replaced by dδ, and thus CTOA in Eq. (1) can be expressed as:

$$\tan\left(\frac{\psi}{2}\right) = \frac{d\delta}{2da} \tag{6}$$

Substitution of Eqs. (4) and (5) into Eq. (6) obtains the following relationship:

$$\tan\left(\frac{\psi}{2}\right) = \frac{2 r_p b}{S}\frac{d\Delta}{da} \tag{7}$$

Differentiation of Eq. (3) yields the following differential load:

$$dP = -\frac{2\lambda \sigma_f B b}{S} da \tag{8}$$

From Eqs. (7) and (8), after eliminating crack extension da, CTOA is obtained as a function of load and the slope of the load-LLD curve:

$$\tan\left(\frac{\psi}{2}\right) = -\frac{4 r_p P}{S}\frac{d\Delta}{dP} \tag{9}$$

When $\psi \le 20^o$, $\tan(\psi/2) \approx \psi/2$ with an error less than 1%.

Assuming the crack steadily grows from Point 1 (P_1, Δ_1, a_1) to Point 2 (P_2, Δ_2, a_2) on the P-LLD curve after the peak load, and CTOA maintains a constant critical value (i.e., ψ_c) during the stable crack growth. In this case, Equation (9) will further derive three load-LLD based CTOA models, as given below.

- **Model 1: P-LLD linear fit model**

Consider a linear portion of measured P-LLD data between Point 1 and Point 2. A linear curve fit of P-LLD data of interest can be expressed as:

$$P = k\Delta + c \tag{10}$$

where k and c are curve-fit constants. Substituting Eq. (10) into Eq. (9) obtains:

$$\tan\left(\frac{\psi_c}{2}\right) = -\frac{4r_p}{S}\left(\Delta + \frac{c}{k}\right) \tag{11}$$

- **Model 2: Ln(P)-LLD linear fit model**

Denote the peak load point (P_{max}, Δ_{max}) on the P-LLD curve. Equation (9) is rewritten as:

$$\tan\left(\frac{\psi_c}{2}\right) = -4r_p \frac{d(\Delta-\Delta_{max})/S}{d\left(Ln\left(\frac{P}{Pmax}\right)\right)} \tag{12}$$

Using the linear regression to fit the linear portion of logarithmic load-LLD data from Point 1 to Point 2, Eq. (12) can be used to calculate ψ_c. If $\psi_c \leq 20^o$, $\tan(\psi_c/2) \approx \psi_c/2$, and Eq. (12) reduce to Eq. (2), as used by ASTM E3039 for DWTT specimens. Zhu et al. [27] further demonstrated that the ln(P)-LLD linear fit model is equivalent to an absorbed stable tearing energy model.

- **Model 3: Ln(P)-LLD polynomial fit model**

Rewrite Eq. (9) in a functional form of ln(P) – LLD as:

$$\tan\left(\frac{\psi}{2}\right) = -\frac{4r_p}{S}\frac{d\Delta}{d(\ln(P))} \tag{13}$$

where a polynomial function of the ln(P) – LLD data is the best-fitted curve from Point 1 to Point 2. Note that all three load-LLD models need only the rotation factor r_P, but not the λ parameter.

3.2. J-differential estimation

In a fracture test, the J-integral resistance curve is evaluated using the incremental J-integral equation as given in ASTM E1820 [6], where measured load, LLD and crack length data are needed for a growing crack. For a quasi-statically growing crack, the differential of the J-integral is obtained as [29]:

$$dJ = \frac{\eta}{Bb}Pd\Delta - \gamma\frac{J}{b}da \tag{14}$$

where η and γ are two LLD-based geometrical factors and a function of a/W for a specimen.

From Eq. (14), the slope of LLD-*a* curve, $d\Delta/da$, can be determined. Coupling with Eq. (7), one obtains the following J-differential equation for determining CTOA:

$$\tan\left(\frac{\psi}{2}\right) = \frac{2r_p}{\eta\lambda\sigma_f}\left(\frac{dJ}{da} + \frac{\gamma}{b}J\right) \tag{15}$$

This is CTOD **Model 4** proposed by Zhu et al. [27].

For standard SENB specimens, it is often taken that $\eta = 2$ and $\gamma = 1$. Note that no assumption of constant CTOA was made in the derivation of Eq. (15). Thus, the J-differential estimate method should be applicable to any crack growth, provided that the large or fully-plastic condition is reached.

4. FRACTURE RESISTANCE TESTING USING SENB

4.1. Fracture resistance testing for X80

Six SENB specimens were tested by Shen et al. [30] at room temperature (about 20 °C) for determining J-R curves for X80 pipeline steel in guidance of ASTM E1820 [6], where initial crack lengths were varied to achieve different constraint levels at the crack tip. These SENB specimens were machined from 48-in X80 pipe. The tensile test obtained the 0.2% offset yield stress of 570 MPa (82.7 ksi) and the ultimate tensile stress (UTS) of 675 MPa (97.9 ksi), leading to the flow stress (σ_f) = 622.5 MPa (90.3 ksi) and Y/T = 0.844 (indicating X80 is a low strain hardening steel). In addition, the Young's modulus is 207 GPa (30,000 ksi), and the Poisson ratio is 0.3.

All SENB specimens have a width W = 23 mm, thickness B = W/2 = 11.5 mm, net thickness B_N = 9.2 mm due to a 10% side groove on each side, and the beam span S = 4W = 92 mm. These SENB specimens were pre-cracked by fatigue in three-point bending. After pre-cracking, the initial crack ratios, a_0/W, of the SENB specimens were 0.24, 0.25, 0.42, 0.43, 0.63, and 0.64.

Figure 3 shows the experimental raw data of load - LLD for six X80 SENB specimens with a_0/W = 0.24 to 0.64 [30]. As shown in Fig. 3, all SENB specimens initially experience linear elastic response, where the load linearly increases with LLD. Then, plastic strain hardening is followed with nonlinearly increasing load up to the peak load. After that, the applied load drops until specimen failure. The load-bearing capacity of these SENB specimens decreases dramatically as the initial crack length increases. For the shallow crack of a_0/W = 0.24, the peak load P_{max} = 32.2 kN. For the intermediate crack of a_0/W = 0.42, P_{max} = 18.6 kN. For the deep crack of a_0/W = 0.63, P_{max} = 7.5 kN.

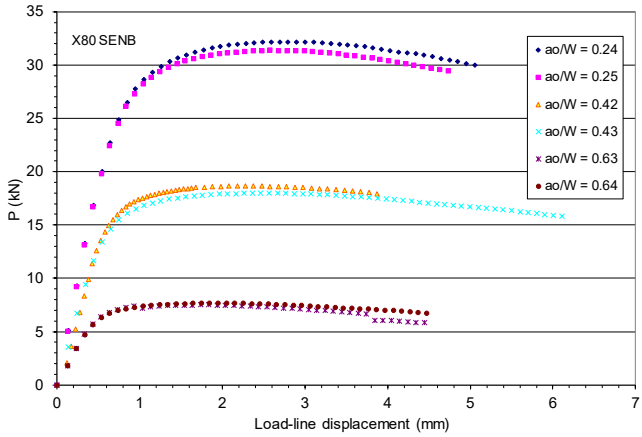

Figure 3. Experimental P–LLD data for six X80 SENB specimens.

Figure 4 shows the experimental J–R curves [30] that were determined following the ASTM E1820 procedures from the load, LLD and crack length, where the crack length was measured using the elastic compliance method. Figure 4 clearly shows a specimen size-dependent or in-plane constraint effect on the J-R curves for the X80 pipeline carbon steel.

Initially, this paper intends to use experimental P-LLD data and J-R curves for X80 to evaluate the above-proposed CTOA methods. However, Figure 4 shows that the crack extensions in all X80 SENB testing are short and the stable crack growth may be less than 0.5 mm for the deep cracks. Thus, these X80 SENB test data are not adequate for a CTOA evaluation.

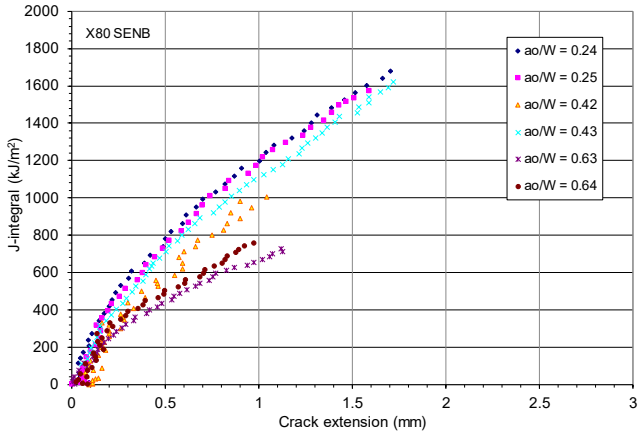

Figure 4. Experimental J–R curves for six X80 SENB specimens.

4.2. Fracture resistance testing for HY80

As an alternate to X80 pipeline steel, HY80 structural steel is considered here because both steels have the same minimum nominal yield stress of 80 ksi (552 MPa). HY80 is a high yield strength submarine steel with low carbon and low alloy and has been used for shipbuilding for more than 55 years [32].

A series of fracture toughness testing results was reported by Joyce and Link [31] for HY80 steel. All fracture tests were conducted on SENB specimens at room temperature (21 ºC) in guidance of ASTM E1820 [6], where initial crack lengths were varied from shallow to deep for developing different constraint levels at the crack tip. The SENB specimens were machined from 27-mm thick plate in HY80 steel. The tensile test obtained the 0.2% offset yield stress of 630 MPa (91.4 ksi) and the UTS of 735 MPa (106.6 ksi), leading to the flow stress (σ_f) = 682.5 MPa (99.0 ksi) and Y/T = 0.857 (indicating HY80 is also a low strain hardening steel). In addition, the Young's modulus is 207 GPa (30,000 ksi), and the Poisson ratio is 0.3.

All SENB specimens have a 1T standard specimen width W = 50.8 mm (2 in.), thickness B = W/2 = 25.4 mm (1 in.), net thickness B_N = 20.32 mm (0.8 in.) due to a total 20% side groove, and the beam span S = 4W = 203 mm (8 in.). These SENB specimens were pre-cracked by fatigue in three-point bending. After pre-cracking, the initial crack ratios, a_0/W, of the SENB specimens were varied in the range of 0.135 to 0.83. This interval represents very shallow to deep cracks and simulates different constraint levels at the crack tip. In general, deep cracks in SENB represent high constraint levels at the crack tip, and shallow cracks in SENB represent low constraint levels at the crack tip.

Figure 5 shows the experimental raw data of load - LLD for 13 HY80 SENB specimens with a_0/W = 0.135 to 0.83 [31]. As shown in Fig. 5, all SENB specimens initially experience linear elastic response, where the load linearly increases with LLD. Then, plastic strain hardening is followed with nonlinearly increasing load up to the peak load. After that, the applied load drops until specimen failure. The load-bearing capacity of these SENB specimens decreases dramatically as the initial crack length increases. For example, the peak load P_{max} = 180.2 kN for the shallow crack of a_0/W = 0.136, the peak load drops to P_{max} = 91.8 kN for the intermediate crack of a_0/W = 0.393, and the peak load fast drops to P_{max} = 37.3 kN for the deep crack of a_0/W = 0.606.

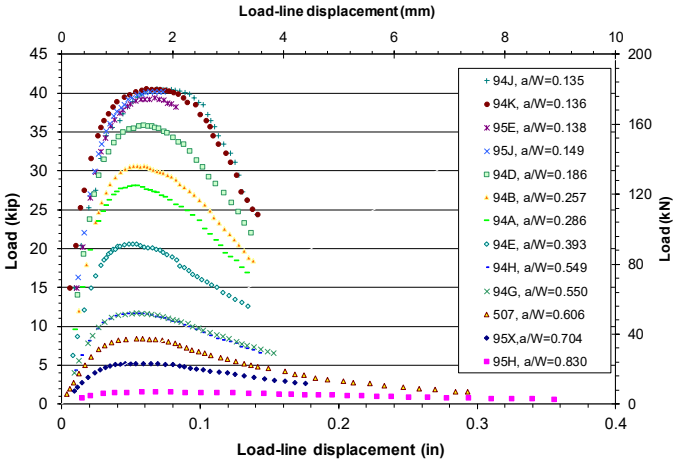

Figure 5. Experimental P–LLD data for a set of HY80 SENB specimens.

In the original fracture toughness testing using HY80 SENB specimens, the unloading compliance method as recommended by ASTM E1820 [6] was adopted for monitoring crack length and determining crack extension. Experimental J-R curves were developed and reported by Joyce and Link [31] for all HY80 SENB specimens. Note that their J-R curves for shallow-cracked SENB specimens with $a_0/W \leq 0.282$ may be incorrect because a negative γ factor was used for the shallow cracks. In the J-R curve evaluation process described by ASTM E1820 [6], the η factor equation is used for calculating incremental deformation J-integral at the current load step, and the γ factor is used for crack growth correction on the increment of the J-integral. This implies that the γ factor must be positive because a negative γ factor increases the deformation J-integral without any physical meaning, see Reference [33] for more discussions. Because of this reason, the original J-R curves are not reported here.

Ten years later, Zhu and Joyce [33] revisited the fracture toughness testing on HY80 SENB specimens and redetermined the crack lengths and J-R curves using the normalization method as recommended in Annex 15 of ASTM E1820 [6]. Note that

more accurate expression of the η factor was developed, and a non-negative expression of the γ factor was obtained by Zhu and Joyce [33]. These new expressions of the η and γ factors were used in the J-R curve reevaluations. Figure 6 shows the experimental J–R curves that were determined by Zhu and Joyce [33] by following the ASTM E1820 procedures from the load, LLD and crack length, where the crack length was estimated using the normalization method. Figure 6 clearly shows a specimen size-dependent or in-plane constraint effect on the J-R curves for the HY80 steel. Recall that ASTM E1820 [6] requires standard SENB specimens having initial crack sizes in the range of $0.45 \le a_0/W \le 0.7$. Figure 6 shows that all non-standard SENB specimens with $a_0/W < 0.45$ or $a_0/W > 0.7$ determined elevated J-R curves compared to the standard J-R curves for SENB specimens with $a_0/W = 0.549$ and 0.606.

Since the crack extensions for HY80 SENB specimens shown in Fig. 6 are larger than 7 mm, these SENB tests data would be adequate for a constant CTOA evaluation against a longer stable ductile crack growth.

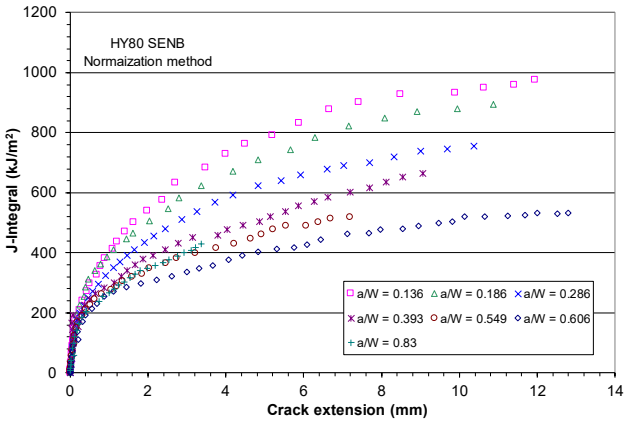

Figure 6. Experimental J–R curves for a set of HY80 SENB specimens.

5. CONSTANT CTOA DETERMINATION FOR HY80

5.1. Determination of λ parameter

In Eq. (15), the J-differential method requires the value of λ parameter for calculating CTOA over stable crack extension. The λ parameter in Eq. (3) is an assumed constant for a perfectly plastic material but may depend on the strain hardening exponent of materials generally. The λ parameter can be estimated from applied load and crack size data measured during fracture testing. From the experimental data, the λ parameter is calculated for each specimen during the entire deformation, as shown in Fig. 7. In this figure, the calculated λ value varies from 1.0 to 2.0 during the plastic deformation and is nearly independent of crack sizes. Figure 5 shows that for all SENB tests, LLD = 2.4 mm corresponds a stable crack growth state that a linear relation exists between load and LLD. At this LLD, from Fig. 7, λ = 1.525 is estimated for use in this work for the HY80 steel.

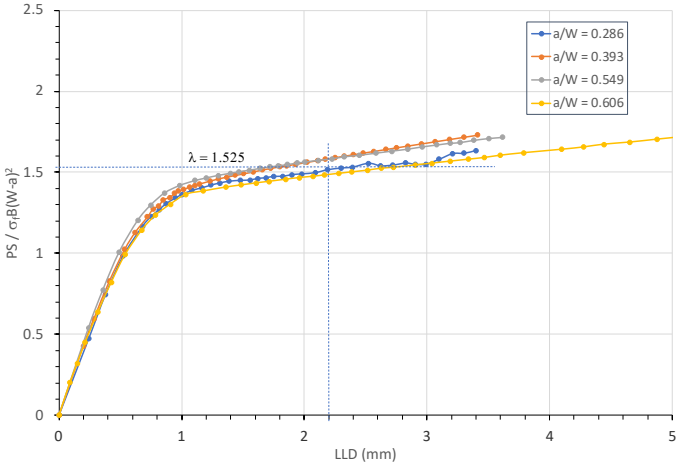

Figure 7. Variation of λ parameter with LLD for four HY80 SENB specimens.

Figure 8 shows variations of the applied load P and the limit load solution in Eq. (3) with the ligament size $(1\text{-}a/W)^2$ during the entire deformation, including initial elastic deformation and plastic deformation during crack growth. Note that in Fig. 8, both the applied and limit loads are normalized using $\sigma_f BW^2/S$. This figure includes two limit load solutions, one uses the estimated λ = 1.525 for HY80 steel, and the other uses λ = 1.455 for a perfect plastic material in the plane strain condition. For each HY80 SENB specimen, the normalized applied load fast increases from small values in the elastic deformation conditions to the maximum values at the full plastic deformation conditions, and then decreases gradually in a linear manner due to stable crack growth. The crack growth direction is marked in Fig. 8. Clearly, the limit load solution with λ = 1.525 is better to match the experimental data and to describe the large-scale yielding or fully plastic conditions for HY80 SENB specimens compared to λ = 1.455 for the perfectly plastic material. Therefore, λ = 1.525 is selected to use hereafter.

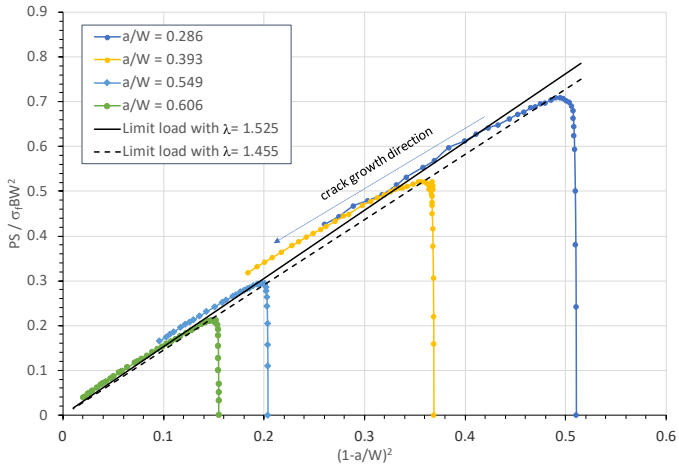

Figure 8. Comparison of limit load with experimental data for four HY80 SENB specimens.

5.2. CTOA for HY80 SENB with $a_0/W = 0.606$

This section determines the critical CTOA value for each HY80 SENB specimen in this section using the P-LLD linear fit model in Eq. (11), the Ln(P)-LLD linear fit model in Eq. (12), the Ln(P)-LLD polynomial fit model in Eq. (12), and the J-differential model in Eq. (15). To quantify the constraint effect on the critical CTOD, four HY80 SENB tests are selected and analyzed in this section. This includes the crack sizes of a_0/W = 0.606, 0.549, 0.393, and 0.286 for HY80 SENB testing. These four crack sizes reflect different constraint effects on J-R curves, as shown in Fig. 6, and describe high to low constraint levels at the crack tip for the HY80 SENB specimens.

In general, experimental raw data contain variations due to measurement noises, and so a smoothed best-fit curve is needed for determining the first-order derivative of the best-fit curve. For the P-LLD linear fit model, the linear curve fit is used to simply fit the experimental data exhibiting a linear relation on the measured P-LLD curve, and then CTOA is calculated from Eq. (11). For the Ln(P)-LLD linear fit model, the peak load point (P_{max}, Δ_{max}) is first located, and then Ln(P/P_{max}) and (Δ-Δ_{max})/S are calculated from the peak load point to the final measured point. The linear regression is used to fit the linear portion of Ln(P/P_{max}) versus (Δ-Δ_{max})/S data, and then CTOA is calculated from Eq. (12). For the Ln(P)-LLD polynomial fit model, Ln(P) is first calculated, and a quadratic or 2-degree polynomial function is curve fitted on the Ln(P)-LLD data. The first-order derivative of the quadratic curve is calculated, and then CTOA is determined from Eq. (13). For the J-differential model, a general 3- or 4-degree polynomial curve is first curve fitted using the nonlinear regression method from an experimental J-R curve. The first-order derivative of the polynomial J-R curve is calculated, and then CTOA is determined from Eq. (15).

Using the above-noted procedures, CTOA resistance curves (or constant CTOA values) against stable crack growth can be determined using the three load-LLD models and the J-differential model. Figure 9 shows the CTOA resistance curves against crack extension, and the CTOA values are obtained using the P-LLD linear fit, the Ln(P)-LLD linear fit, the Ln(P)-LLD polynomial fit, and the J-differential models, respectively for the HY80 SENB specimen with the deep crack of a_0/W=0.606. It is seen that all proposed models determine comparable critical CTOA values over the range of stable crack extension from Δa = 2.0 mm to 6.2 mm. It is observed that over the stable crack growth zone: (1) the Ln(P)-LLD linear fit model determines a constant CTOA, ψ_c = 3.21°, (2) the P-LLD linear fit model determines a linearly decreasing CTOA with an average value of ψ_c = 3.18°, (3) the Ln(P)-LLD polynomial fit model determines a nonlinearly decreasing CTOA with an average value of ψ_c = 3.25°, (4) the J-differential model can determine CTOA over a large crack growth, and the CTOA curve becomes nearly flat over the stable crack growth zone with an average value of ψ_c = 3.18°, and (5) the J-differential model is similar to the Ln(P)-LLD polynomial fit over the stable crack growth.

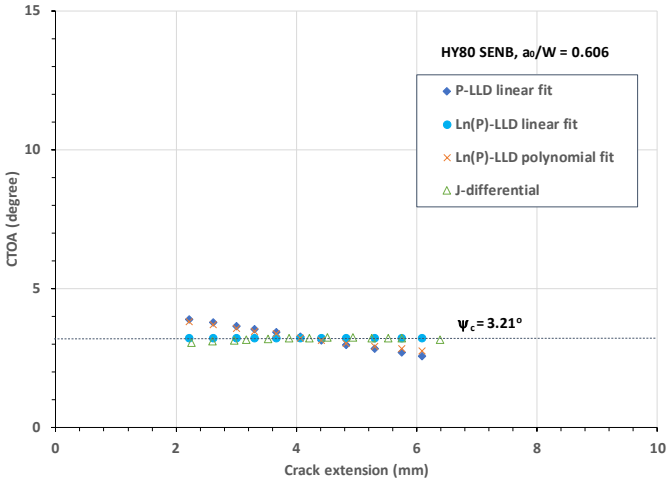

Figure 9. CTOA resistance against crack growth for HY80 SENB specimen with a_0/W = 0.606.

5.3. CTOA for HY80 SENB WITH $a_0/W = 0.549$

In the same manner as used above, four best curve-fitted functions are obtained and then utilized to calculate CTOA values in conjunction with use of the load-displacement models and the J-differentiation model. Figure 10 shows the CTOA resistance against crack extension obtained using the P-LLD linear fit, the Ln(P)-LLD linear fit, the Ln(P)-LLD polynomial fit, the J-differential methods for HY80 SENB specimen with the deep crack of a_0/W=0.549.

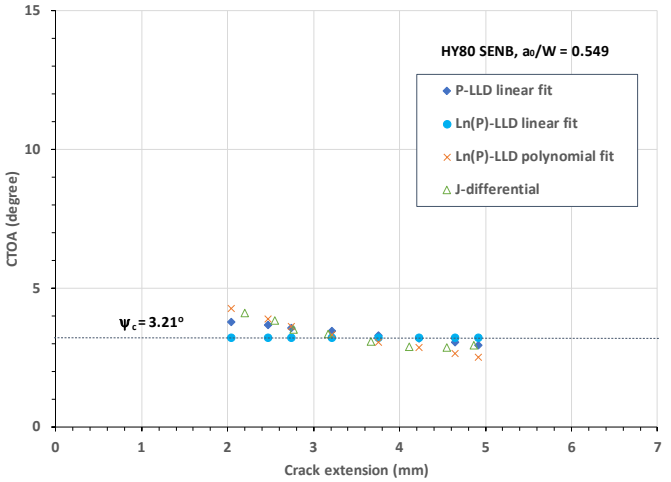

Figure 10. CTOA resistance against crack growth for HY80 SENB specimen with a_0/W = 0.549.

As evident in Fig. 10, all CTOA models determine comparable critical CTOA values over the range of stable crack growth from Δa = 2.0 mm to 5.0 mm. Figure 10 shows that over the stable crack growth zone, (1) the Ln(P)-LLD linear fit model determines a constant CTOA, ψ_c = 3.21°, (2) the P-LLD linear fit model determines a linearly decreasing CTOA with an

average value of ψ_c = 3.36°, (3) the Ln(P)-LLD polynomial fit model determines a nonlinearly decreasing CTOA with an average value of ψ_c = 3.27°, (4) the J-differential model determines nearly constant CTOA over the stable crack growth zone with an average value of ψ_c = 3.21°, and (5) the J-differential model is similar to the ln(P)-LLD polynomial fit over the stable crack extension.

5.4. CTOA for HY80 SENB WITH a_0/W = 0.393

In the same manner as used in two subsections above, four best curve-fitted functions are obtained and employed to determine the CTOA values in conjunction with use of the two load-displacement models and the J-differentiation model. Figure 11 shows the CTOA resistance against crack extension obtained from the P-LLD linear fit, the Ln(P)-LLD linear fit, the Ln(P)-LLD polynomial fit, and the J-differential methods, respectively for HY80 SENB specimen with an intermediate crack size of a_0/W=0.393.

Figure 11 shows that all CTOA estimate models determine comparable critical CTOA values over the stable crack extension from Δa = 3.8 mm to 8.1 mm. From Fig. 11, it is observed that over the stable crack growth zone, (1) the Ln(P)-LLD linear fit model determines a constant CTOA, ψ_c = 3.62°, (2) the P-LLD linear fit model determines a linearly decreasing CTOA with an average constant value of ψ_c = 3.63°, (3) the Ln(P)-LLD polynomial fit model determines an almost linearly decreasing CTOA with an average value of ψ_c = 3.65°, (4) the J-differential model determines a nearly constant CTOA over the stable crack growth zone with an average constant value of ψ_c = 3.51°, and (5) the J-differential model determines lower CTOA values over most area of stable crack extension. These lower CTOA values may be caused by use of the constant η = 2 for all crack sizes of HY80 SENB specimens because this η value was used in the experimental J-R curve evaluation [31]. If a smaller η value is used, the CTOA value will go up somehow.

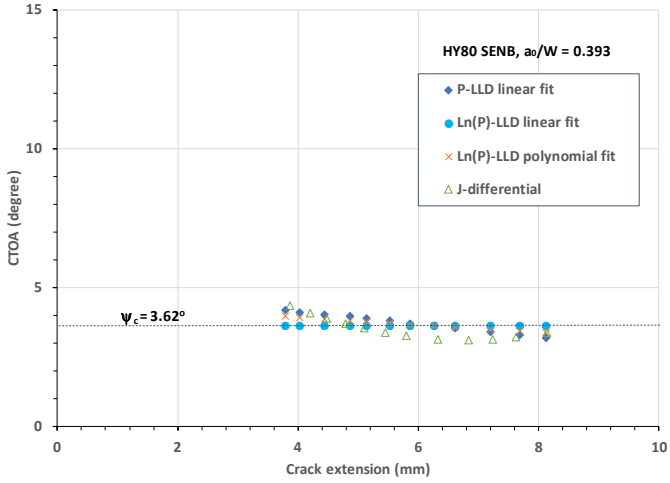

Figure 11. CTOA resistance against crack growth for HY80 SENB specimen with a_0/W = 0.393.

5.5. CTOA for HY80 SENB WITH a_0/W = 0.286

In the similar way, Figure 12 shows the CTOA resistance against crack extension obtained from the P-LLD linear fit, the Ln(P)-LLD linear fit, the Ln(P)-LLD polynomial fit, and the J-differential methods, respectively for HY80 SENB specimen with a shallow crack size of a_0/W=0.286.

Figure 12 shows that all CTOA estimate models determine comparable critical CTOA values over the stable crack extension from Δa = 3.2 mm to 7.0 mm. From Fig. 12, it is observed that over the stable crack growth zone, (1) the Ln(P)-LLD linear fit model determines a constant CTOA, ψ_c = 3.19°, (2) the P-LLD linear fit model determines a linearly decreasing CTOA with an average constant value of ψ_c = 3.21°, (3) the Ln(P)-LLD polynomial fit model determines a nonlinearly decreasing CTOA with an average value of ψ_c = 3.22°, (4) the J-differential model determines a nonlinearly decreasing CTOA with an average constant value of ψ_c = 3.19°, and (5) the J-differential model determines a CTOA trend similar to the Ln(P)-LLD polynomial fit model. Note that η = 2 was used in the original experimental J-R curve evaluation for this shallow crack. In fact, the η factor for this shallow crack is not a constant but varies with the crack extension.

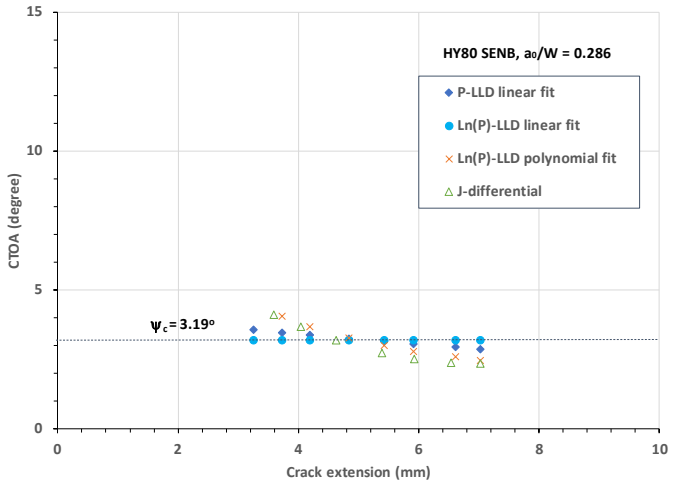

Figure 12. CTOA resistance against crack growth for HY80 SENB specimen with a_0/W = 0.286.

In summary, the above analyses, as shown in Figs. 9-12, demonstrate that (1) the Ln(P)-LLD linear fit model determines a constant CTOA over the stable crack growth for the shallow and deep cracks of HY80 SENB specimens, (2) the P-LLD linear fit model determines a linearly decreasing CTOA over the stable crack growth for all cracks, (3) the Ln(P)-LLD polynomial fit model determines a nonlinearly decreasing CTOA over the stable crack growth for all cracks, and (4) the J-differential model may determine a constant or nonlinearly decreasing CTOA over the stable crack growth. The result depends on the quality of experimental J-R curve test data and the polynomial curve fit over the entire range of crack extension.

5.6. Constraint independence of critical CTOA

Figure 13 compares the constant critical CTOA values with crack sizes for the HY80 SENB specimens. As shown in Fig. 13, the crack size or crack-tip constraint level has a small or negligible effect on the critical CTOA value, and the averaged critical CTOA = 3.32° for the HY80 steel. In contrast, the crack-tip constraint level has a significant effect on the J-R curves for the HY80 steel, as shown in Fig. 6.

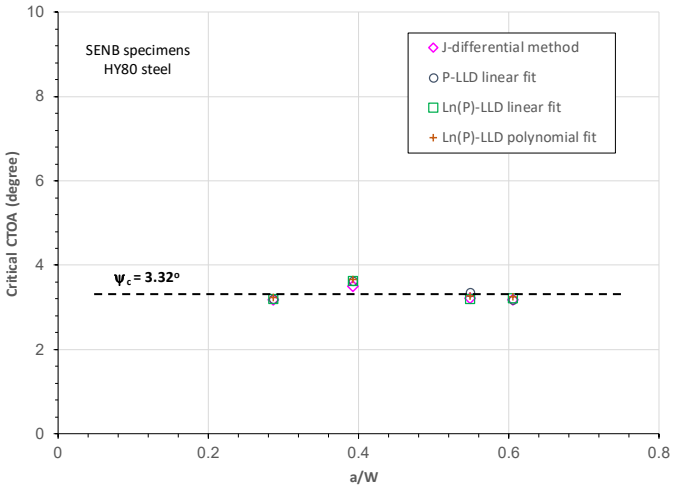

Figure 13. Variations of critical CTOA with crack sizes for HY80 SENB specimens.

6. CONCLUSIONS

This paper evaluated four CTOA estimate models for estimating the critical CTOA over stable crack growth using SENB specimens. A set of fracture test data on SENB specimens for HY80 structural steel were employed to assess the proposed CTOA models and to evaluate the critical CTOA for HY80 steel. The major results are summarized as:

1) The Ln(P)-LLD linear fit model determined a constant critical CTOA over stable crack growth. The P-LLD linear fit model determines a linearly decreasing CTOA, and the Ln(P)-LLD polynomial fit model determines a nonlinearly decreasing CTOA over stable crack growth. On average, these three load-displacement models determined the nearly identical CTOA values over stable crack growth.

2) Using experimental J-R curve data, the J-differential method determined comparable critical CTOA values over stable crack growth.

3) The results showed that the Ln(P)-LLD linear fit model, as used by ASTM E3039, determined a constant CTOA over the stable crack growth for all crack sizes. The other three CTOA models also determined comparable critical CTOA.

4) The results demonstrated that the critical CTOA determined using HY80 SENB specimens is independent of crack size or constraint level at the crack tip. This infers that CTOA measured by ASTM E3039 is constraint-independent, and thus supports the transferability of CTOA measured by ASTM E3039 to an actual crack assessment.

ACKNOWLEDGEMENTS

This document was prepared in conjunction with work accomplished under Contract No. 89303321CEM000080 with the U.S. Department of Energy (DOE) Office of Environmental Management (EM).

REFERENCES

[1] Rice JR, "A Path Independent Integral and the Approximate Analysis of Strain Concentration by Notches and Cracks," *Journal of Applied Mechanics*, Vol. 35, 1968: 379-386.

[2] Wells AA, "Application of Fracture Mechanics at and beyond General Yielding," *British Welding Journal*, Vol. 10, 1963: 563-570.

[3] Anderson H, "A Finite Element Representation of Stable Crack Growth," *Journal of Mechanics and Physics in Solids*, Vol. 21, 1973: 337-356.

[4] Zhu X-K, Joyce JA, "Review of Fracture Toughness (G, K, J, CTOD, CTOA) Testing and Standardization," *Engineering Fracture Mechanics*, Vol. 85, 2012: 1-46.

[5] ASTM E399-22, *Standard Test Method for Linear-Elastic Plane-Strain Fracture Toughness of Metallic Materials*. American Society of Testing and Materials International, West Conshohocken, PA, 2022.

[6] ASTM E1820-21, *Standard Test Method for Measurement of Fracture Toughness*. American Society of Testing and Materials International, West Conshohocken, PA, 2022.

[7] Zhu X-K, "Review of Fracture Toughness Test Methods for Ductile Materials in Low-Constraint Conditions," *International Journal of Pressure Vessels and Piping*, Vol. 139-140, 2016: 173-183.

[8] Newman JC, James MA, Zerbst U, "A Review of the CTOA/CTOD Fracture Criterion," *Engineering Fracture Mechanics*, Vol. 70, 2003: 371-385.

[9] ASTM E2472-12e1, *Standard Test Method for Determination of Resistance to Stable Crack Extension under Low-Constraint Conditions*, American Society of Testing and Materials International, West Conshohocken, PA, 2018.

[10] Chao YJ, Sutton MA, "Accurate Measurement of Two- and Three-Dimensional Surface Deformations for Fracture Specimens by Computer Vision," *Experimental Techniques in Fracture* (editor: J.S. Epstein), VCH Publisher, 1993: 59-94.

[11] Darcis PP, McCowan CN, Windhoff H, McCloskey JD, Siewer TA, "Crack Tip Opening Angle Optical Measurement Methods in Five Pipeline Steels," *Engineering Fracture Mechanics*, Vol. 75, 2008: 2453-2468.

[12] Horsley DJ, "Background to the Use of CTOA for Prediction of Dynamic Ductile Fracture Arrest in Pipelines," *Engineering Fracture Mechanics*, Vol. 70, 2003: 547-552.

[13] Zhu X-K, "State-of-The-Art Review of Fracture Control Technology for Modern and Vintage Gas Transmission

Pipelines," *Engineering Fracture Mechanics*, Vol. 148, 2015: 260-280.

[14] Tyson WR, Newman JC, Xu S, "Characterization of Stable Ductile Crack Propagation by CTOA: Review of Theory and Applications," *Fatigue and Fracture in Engineering Materials and Structures*, Vol. 41, 2018: 2421-2437.

[15] Ben Amara M, Pluvinage G, Cappelle J, Azari Z, "New Numerical Tools to Calibrate the Two Curves Method Using the CTOA Criterion," *Engineering Fracture Mechanics*, Vol. 205, 2019: 532-546.

[16] Xu S, Bassindale C, Xue J, Williams BW, Wang X, "Recent Progress in Development of Ductile Fracture Arrest Methodology Based on CTOA: Test Standard, Transferability and Methodology," *Proceedings of the 13th International Pipeline Conference*, September 29-30, 2020, Virtual, Online. IPC2020-9299.

[17] Zhen Y, Zu Y, Cao Y, Niu R, "Effect of Accurate Prediction of Real-Time Crack Tip Position on Dynamic Crack Behaviors in Gas Pipeline," *Journal of Natural Gas Science and Engineering*, Vol. 94, 2021: 104136.

[18] Bassindale C, Wang X, Tyson WR, Xu S, Guan C, Rothwell B, "Analysis of Full-Scale Burst Test by FE Modelling Using Constant CTOA Fracture Criterion," *Journal of Pipeline Science and Engineering*, Vol. 2, 2022: 52-59.

[19] Xu S, Eagleson R, Tyson WR, Park D-Y. "Cracking Tunnelling and Crack Tip Opening Angle in Drop-Weight Tear Test Specimens," *International Journal of Fracture*, Vol. 172, 2011: 105-112.

[20] Xu S, Simha CHM, William BW, Tyson WR, "CTOA Testing of Thick DWTT Specimens: Experiment and FEA Simulation for Development of An Annex for ASTM E3039," *Journal of Testing and Evaluation*, Vol. 48(6), 2020: JTE20180816.

[21] Martinelli A, Venzi S, "Tearing Modulus, J-integral, CTOA and Crack Profile Shape Obtained from the Load-Displacement Curve Only," *Engineering Fracture* Mechanics, Vol. 53, 1996: 263-277.

[22] Xu S, Bouchard R, Tyson WR, "Simplified Single-Specimen Method for Evaluating CTOA," *Engineering Fracture Mechanics*, Vol. 74, 2007: 2459-2464.

[23] ASTM E3039-20, *Standard Test Method for Determination of Crack Tip Opening Angle of Pipe Steels using DWTT Specimens*, American Society of Testing and Materials International, West Conshohocken, PA, 2020.

[24] Xu S, Tyson WR, Eagleson R, "Measurement of CTOA of Pipeline Steels using MDCB and DWTT Specimens," *Proceedings of the 8th International Pipeline Conference*, September 27 – October 1, 2010, Calgary, Alberta, Canada. IPC2010-31076.

[25] Gullerud AS, Dodds RH, Hampton RW, Dawicke DS, "Three-Dimensional Modeling of Ductile Crack Growth in Thin Sheet Metals: Computational Aspects and Validation," *Engineering fracture Mechanics*, Vol. 63, 1999: 347-374.

[26] Shuai J, Tu S, Wang J, Ren X, He J, Zhang Z, "Determination critical CTOD for Energy-Load Curves with DWTT Specimen," *Engineering Fracture Mechanics*, Vol. 186, 2017: 47-58.

[27] Zhu X-K, Lam P-S, Chao YJ, "Constraint-dependent CTOA determination for stable ductile crack growth," *Engineering Fracture Mechanics*, Vol. 271, 2022: 108651.

[28] BS 7448-1, *Fracture Mechanics Toughness Tests – Part 1: Method for Determination of K_{IC}, Critical CTOD, and Critical J Values of Metallic Materials*, British Standards Institution, 1991.

[29] Zhu X-K, "Improved Incremental J-Integration Equations for Determining Crack Growth Resistance Curves," *Journal of Pressure Vessel Technology*, Vol. 134, 2012: 051404.

[30] Shen G., Tyson WR, Glover A, Horsley D, "Constraint Effects on Linepipe Toughness," *Proceedings of the 4th International Conference on Pipeline Technology*, Vol. 2, May 9-13, 2004, Ostend, Belgium, pp. 703-720.

[31] Joyce JA, Link RE, "Application of Two Parameter Elastic-Plastic Fracture Mechanics to Analysis of Structures," *Engineering Fracture Mechanics*, Vol. 57, 1997: 431-446.

[32] Bogdan S, Radoslaw K, "Material Properties of HY80 Steel after 55 Years of Operation for FEA Applications," *Materials*, Vol. 14, 2021: 4213.

[33] Zhu X-K, Joyce JA, "J-Resistance Curve of HY80 Steel Using SE(B) Specimens and Normalization Method," *Engineering Fracture Mechanics*, Vol. 74, 2007: 2263-2281.